



# 1     **An improved global zenith tropospheric delay model** 2                   **GZTD2 considering diurnal variations**

3                   YiBin Yao<sup>1,2,3</sup>, YuFeng Hu<sup>1</sup>, Chen Yu<sup>1</sup>, Bao Zhang<sup>1</sup>, JianJian Guo<sup>1</sup>

4                   <sup>1</sup>*School of Geodesy and Geomatics, Wuhan University, 129 Luoyu Road, Wuhan 430079, China. E-*  
5                   *mail: [ybyao@whu.edu.cn](mailto:ybyao@whu.edu.cn)*

6                   <sup>2</sup>*Key Laboratory of Geospace Environment and Geodesy, Ministry of Education, Wuhan University,*  
7                   *129 Luoyu Road, Wuhan 430079, China*

8                   <sup>3</sup>*Collaborative Innovation Center for Geospatial Technology, 129 Luoyu Road, Wuhan 430079,*  
9                   *China*

10

11     **Abstract**--The zenith tropospheric delay (ZTD) is an important atmospheric parameter  
12     in the wide application of GNSS technology in geoscience. Given that the temporal  
13     resolution of the current Global Zenith Tropospheric Delay model (GZTD) is only 24  
14     h, an improved model GZTD2 has been developed by taking the diurnal variations into  
15     consideration and modifying the model expansion function. The data set used to  
16     establish this model is the global ZTD grid data provided by Global Geodetic Observing  
17     System (GGOS) Atmosphere spanning from 2002 to 2009. We validated the proposed  
18     model with respect to ZTD grid data from GGOS Atmosphere, which was not involved  
19     in modeling, as well as International GNSS Service (IGS) tropospheric product. The  
20     obtained results of ZTD grid data show that the global average Bias and RMS for  
21     GZTD2 model are 0.2 cm and 3.8 cm respectively. The global average Bias is  
22     comparable to that of GZTD model, but the global average RMS is improved by 3 mm.  
23     The Bias and RMS are far better than EGNOS model and the UNB series models. The  
24     testing results from global IGS tropospheric product show the Bias and RMS (-0.3 cm  
25     and 3.9 cm) of GZTD2 model are superior to that of GZTD (-0.3 cm and 4.2 cm),  
26     suggesting higher accuracy and reliability compared to the EGNOS model, as well as  
27     the UNB series models.

28     **Key Words**—Zenith tropospheric delay; GGOS Atmosphere; IGS; Diurnal variation;  
29     GZTD2 model.



## 30 1. Introduction

31 Radio space-based geodesy techniques suffer from atmosphere propagation delays,  
32 of which the ionospheric delay can be largely eliminated by iono-free carrier phase  
33 combination techniques, and then the tropospheric delay becomes the main error source.  
34 In general, we project the slant delay to zenith direction with mapping function in GNSS  
35 navigation and positioning, so modeling the ZTD is a common method to reduce the  
36 tropospheric influence on signal travelling. In order to better exploit the modern  
37 development of geodetic techniques, a more reliable tropospheric delay model is  
38 required to improve the accuracy and efficiency of the application in earth science based  
39 on space geodesy techniques.

40 The correction accuracy of some traditional tropospheric delay models such as  
41 Hopfield model (Hopfield 1969), Saastamoinen model (Saastamoinen 1973), Black  
42 model (Black 1978), can be up to centimeter or decimeter level using the real-time  
43 meteorological parameters, while these models perform poorly when using the standard  
44 atmospheric meteorological parameters. Collins and Langley (1997) established UNB  
45 series models for the promotion of U.S. Wide Area Augmentation Navigation System  
46 (WAAS). In North America, the average tropospheric zenith delay error of UNB3  
47 model was 2 cm (Collins et al. 1998). UNB3m model estimates the wet delay using  
48 relative humidity, and the average deviation was -0.5 cm (Leandro et al. 2006; Leandro  
49 et al. 2008). EGNOS model is a tropospheric delay correction model used by European  
50 Geostationary Navigation Overlay System (EGNOS), which is established by using the  
51  $1^\circ \times 1^\circ$  grid data generated by the European Centre for Medium-Range Weather  
52 Forecasts (ECMWF) (Dodson et al. 1999; Penna et al. 2001; Ueno et al. 2001), whose  
53 correction accuracy is close to that of Hopfield and Saastamoinen model provided with  
54 meteorological measurements. Li Wei et al. (2012) established the IGGtrop global  
55 tropospheric delay empirical model using the three-dimensional parameter table from  
56 reanalysis data of National Centers for Environmental Prediction (NCEP), which  
57 considered the longitudinal changes of zenith troposphere. The accuracy was improved  
58 significantly, but the calculation of zenith tropospheric total delay required a number of



59 parameters. Then Li Wei et al. (2015) developed the new versions of IGGtrop named  
60 IGGtrop<sub>ri</sub> (i = 1, 2, 3) by simplifying the algorithm and lowering the resolution, which  
61 substantially reduce the required numbers with a similar accuracy. Krueger (2004;2005)  
62 and Schüller (2014) obtained the annual and diurnal coefficients for underlying  
63 parameters by fitting every grid point's meteorological parameters time series of NCEP  
64 atmospheric data, and established two global tropospheric delay models — TropGrid  
65 and TropGrid2 with resolution of  $1^\circ \times 1^\circ$ . The correction accuracy of TropGrid2 is  
66 slightly better than that of IGGtrop model. Båm et al. (2015) proposed Global pressure  
67 and temperature 2 wet (GPT2w) as an extension to GPT2 (Lagler et al. 2013) with an  
68 improved capability to determine zenith wet delays in blind model. The GPT2w model  
69 account for the annual and semiannual variations of meteorological parameters, and the  
70 validation with IGS data and an extended validation with ray-traced delays (Müller et  
71 al. 2014) show a high accuracy of about 3.6 cm for GPT2w. However, GPT2w has  
72 numerous parameters for storage like above grid models such as IGGTrop series models  
73 and TropGrid series models.

74 Yao et al. (2013) established a global non-meteorological parameters tropospheric  
75 delay model GZTD (Global Zenith Tropospheric Delay) based on spherical harmonics  
76 using the global zenith tropospheric delay grid data provided by Global Geodetic  
77 Observing System (GGOS) Atmosphere. The harmonic function including three terms  
78 (mean, annual and semi-annual) is used to fit the ZTD time series from 2002 to 2009  
79 for each grid, then the fitted coefficients of all the grids are expanded with a 10-order  
80 and 10-degree spherical harmonics. Its modeling approach was very simple, and the  
81 overall accuracy of 4.2 cm was similar to the IGGtrop on a global scale, but the required  
82 parameters were reduced greatly to about 600. GZTD model is constructed by global  
83 daily average ZTD grid data and the model parameters were expanded with a low order  
84 spherical harmonics, whose temporal resolution is only one day in theory and spatial  
85 resolution is low.

86 In this paper, using the ZTD grid data provided by the GGOS Atmosphere, the  
87 diurnal variations in ZTD were analyzed to prove the theoretical necessity for  
88 temporal resolution improvement of GZTD model. Then on the basis of GZTD model



89 and taking the diurnal variations into consideration and modifying the expansion  
90 function, we developed an improved global non-meteorological parameters ZTD model  
91 — GZTD2. The data set used to establish this model is the global ZTD grid data  
92 provided by the GGOS Atmosphere from 2002 to 2009. Using ZTD grid data obtained  
93 from GGOS Atmosphere and tropospheric product (Buyn et al. 2009) provided by IGS  
94 for model validation, the accuracy of GZTD2 model is superior to that of GZTD model,  
95 and this model performs much better than other commonly used models such as  
96 EGNOS model and UNB series models.  
97

## 98 **2 The new tropospheric delay model**

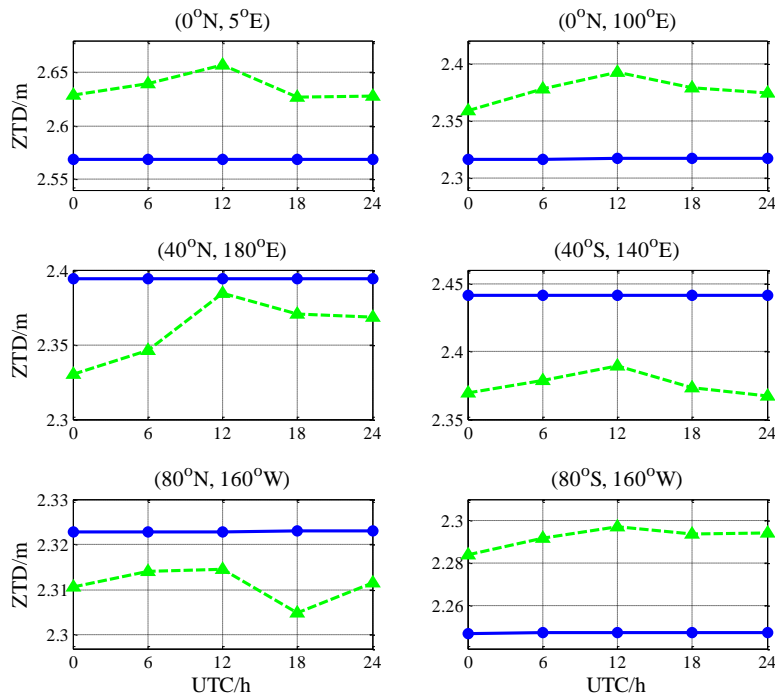
99 The GGOS Atmosphere is a project that aims to establish atmospheric models,  
100 which has been carried out at Vienna University of Technology and has been funded by  
101 the Austrian Science Fund (Böhm & Schuh 2013). It provides grid data of global zenith  
102 delays (including zenith hydrostatic delay (ZHD) and zenith wet delay (ZWD)) with  
103 temporal resolution of 6 hours (0:00, 6:00, 12:00, 18:00UTC) and spatial resolution of  
104  $2.5^\circ \times 2^\circ$  (lon $\times$ lat), which are derived from the reanalysis data (Uppala et al. 2005)  
105 provided by the ECMWF. The ZTD grid data can be obtained by simply adding up the  
106 ZHD and the ZWD at the same point and time. In this paper, the research about model  
107 establishment is based on the ZTD grid data.

### 108 **2.1 Diurnal variations in ZTD**

109 Yao et al. (2013) developed a new global zenith tropospheric delay model (GZTD),  
110 which is based on spherical harmonics without using meteorological parameters. GZTD  
111 model depends on four parameters: the day of year (doy), the latitude, the longitude and  
112 the height; and the overall accuracy is up to centimeter level. However, the algorithm  
113 of GZTD model only considers the annual and semiannual cycles in ZTD and the  
114 establishment of GZTD model is based on the daily average of global grid ZTD data,  
115 hence the temporal resolution of GZTD model is one day (24 h) in theory. We randomly



116 selected six grid points which represent the regions in low, middle and high latitude in  
 117 both the southern and northern hemispheres respectively, and applied GZTD model to  
 118 estimate the ZTD at four moments (0:00,6:00,12:00,18:00 UTC) of the first doy in 2010,  
 119 then compared the GZTD model estimations with the corresponding data from GGOS.  
 120 The results are shown in Figure 1.

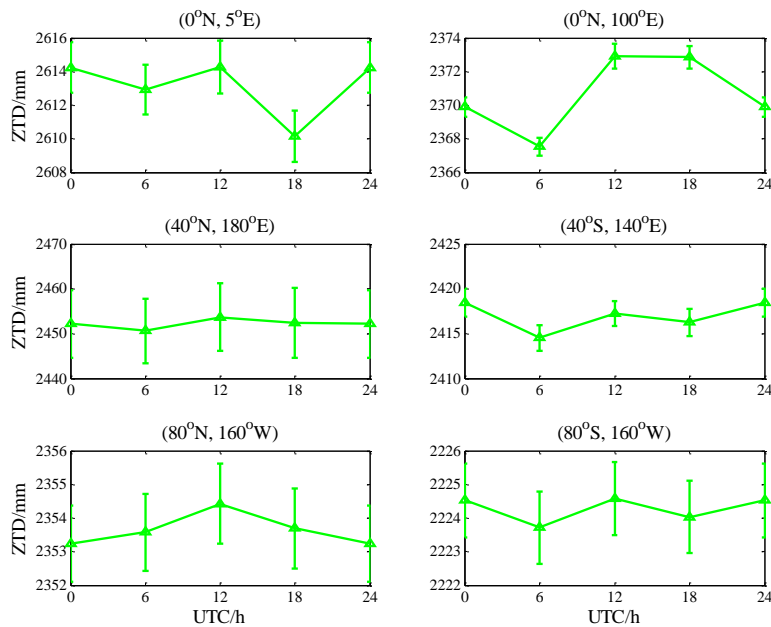


121  
 122 **Figure 1.** GZTD model estimates (blue ○) and corresponding GGOS grid values (green Δ) at the  
 123 first doy of 2010

124 We can see clearly from Figure 1 that the ZTD estimates of GZTD model can  
 125 almost be fitted with a straight line parallel to the time axis which only varies about 1  
 126 mm in a single day. The real variations of GGOS grid ZTD data are mostly up to  
 127 centimeter level, which is one order larger than the variations of GZTD model estimates.  
 128 Furthermore, we calculated the mean diurnal ZTD values of these six GGOS grid points  
 129 over the whole 2010 year (Figure 2), and the significant signal of diurnal variation can  
 130 be seen at all these six grid points. We can draw a conclusion that GZTD model could  
 131 not reflect the characteristic of diurnal variations in ZTD, so the model estimations  
 132 nearly have no difference when doing calculation with real value or corresponding



133 integer value of the input day. Therefore, it is necessary to improve the temporal  
134 resolution of GZTD model to reflect diurnal variations. It should be noted that Jin et al.  
135 (2009) has investigated the diurnal and semidiurnal variations in ZTD which obtained  
136 from a decade of global GPS observations, and thought that the atmospheric tides were  
137 the major driver of these variations after finding the general similarities of diurnal  
138 variations between ZTD and pressure. However, the semidiurnal variations could  
139 hardly be described because of the low temporal resolution (6 h) of GGOS ZTD data,  
140 so we didn't consider the semidiurnal components of ZTD in modeling in the following  
141 section.



142

143 **Figure 2.** Mean diurnal ZTD values of GGOS grid points with error bars over the 2010 year

## 144 2.2 Establishment of GZTD2 model

145 According to the previous researches conducted by Jin et al. (2007) and Yao et al.  
146 (2013), ZTD decreases exponentially with increasing height, and is featured by one-  
147 year periodicity and half-year periodicity, and has a strong correlation with latitude.



148 Based on these characteristics of ZTD, we took diurnal periodic variations into  
149 consideration to develop an improved model GZTD2. The expression of GZTD2 model  
150 is as follows:

$$151 \quad ZTD = \left[ a_0 + a_1 \cos\left(2\pi \frac{\text{doy} - a_2}{365.25}\right) + a_3 \cos\left(4\pi \frac{\text{doy} - a_4}{365.25}\right) + a_5 \cos\left(2\pi \frac{\text{hod} - a_6}{24}\right) \right] \exp(\beta h) \quad (1)$$

152  
153 Where,

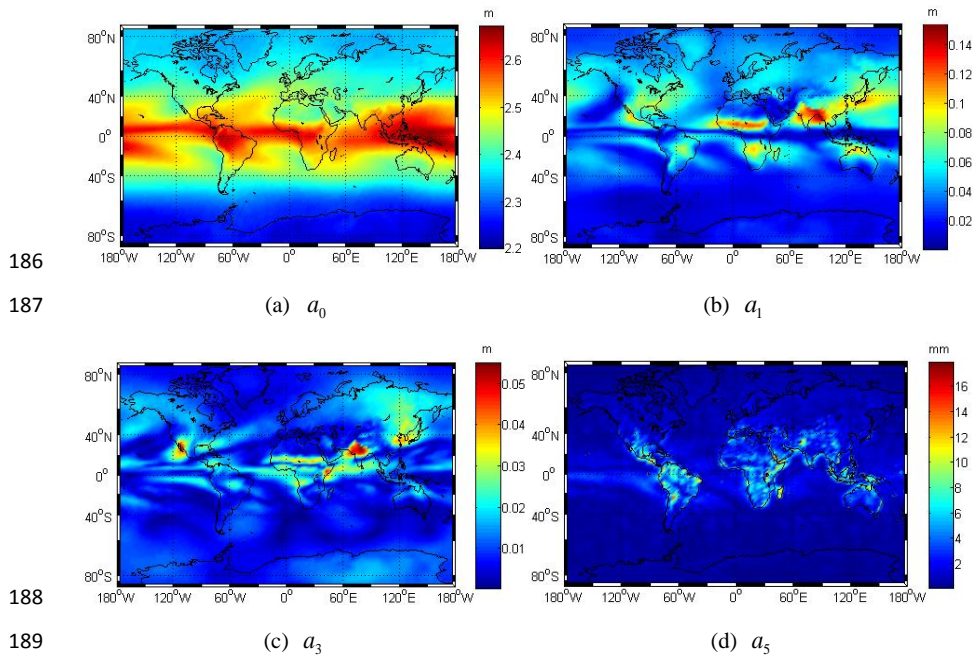
$$154 \quad a_i = \sum_{n=0}^{18} \sum_{m=0}^n P_{nm}(\sin \varphi) \cdot [A_{nm}^i \cos(m\lambda) + B_{nm}^i \sin(m\lambda)] \quad (i = 0, 1, \dots, 6) \quad (2)$$

155 In equation(1), do $y$  is the day of year; hod is the UTC time;  $h$  is the height  
156 (altitude);  $a_0$  is the annual mean of ZTD on the mean sea level (MSL);  $a_1$  is the annual  
157 variation amplitude of ZTD;  $a_2$  is the initial phase of annual variation;  $a_3$  is the  
158 semiannual variation amplitude of ZTD;  $a_4$  is the initial phase of semiannual variation;  
159  $a_5$  is the diurnal periodic variation amplitude of ZTD;  $a_6$  is the initial phase of diurnal  
160 variation;  $\beta = -0.00013137$  is the constant to reduce the ZTD at height to the MSL,  
161 which was determined by Yao et al. (2013) by fitting the global GGOS grid ZTD via  
162 exponential function with respect to height;  $P_{nm}$  is the Legendre polynomials;  $\varphi$  is the  
163 latitude of grid point;  $\lambda$  is the longitude of grid point;  $A_{nm}^i$  and  $B_{nm}^i$  are the  
164 coefficients of spherical harmonics determined by least square optimization.

165 For each grid-point-specific ZTD time series derived from GGOS Atmosphere, we  
166 used equation (1) to fit them to temporal coefficients at MSL. However, there are seven  
167 coefficients for each grid, which need large storage space on global scale. Then  
168 referring to the idea of spherical harmonics used in GPT (Břm et al., 2007), we used  
169 equation (2) to express the temporal coefficients (mean, annual terms et al) of all grids  
170 as a function of location (latitude, longitude and height), thus reducing the parameters.  
171 Different from the GZTD model established using daily average global ZTD data, we  
172 utilized the ZTD time series data of four moments per day (0:00, 6:00, 12:00, 18:00UTC)



173 from 2002 to 2009, provided by GGOS Atmosphere, to fit ZTD values to obtain  
174 temporal variation parameters via equation (1), then expanded these parameters with a  
175 18-order and 18-degree spherical harmonic function (equation (2)), respectively. We  
176 used this spherical harmonic function instead of the 10-order and 10-degree function  
177 adopted in GZTD model because it is not sufficient to apply the previous 10 order  
178 function for the expansion of the temporal variation parameters with relatively high  
179 resolution. The number of order and degree of spherical harmonics determine the  
180 horizontal resolution of model. However, higher order and degree bring more  
181 parameters for model. The resolution of GZTD model is about  $18^\circ$  while the diurnal  
182 variations are mostly less than 5 mm. The 10 spherical harmonics are too low for  
183 GZTD2 model to reflect the diurnal variations. To keep a balance between the  
184 resolution and number of parameters, we used 18 spherical harmonics for GZTD2  
185 whose resolution is about  $10^\circ$ .



190 **Figure 3.** The global distribution of the annual mean ZTD on MSL (a) , the annual variation  
191 amplitude (b), the semiannual variation amplitude (c), and the diurnal variation amplitude (d)  
192 Figure 3 shows the global distributions of the annual mean of ZTD on MSL and



193 amplitude parameters after fitting by equation (1). As can be seen from Figure 3a, the  
194 coefficient  $a_0$  in low latitudes, especially, near the equator, are significantly larger  
195 than that in high latitudes, and the distribution in the Southern Hemisphere is more  
196 uniform than that in the Northern Hemisphere; These results are mostly in agreement  
197 with the results of Li et al. (2012) and Yao et al. (2013). For the sawtooth shape in the  
198  $40^\circ\text{N}$ - $40^\circ\text{S}$  region, Yao et al. (2013) found this shape appear in coastal areas and is  
199 consistent with the directions of equatorial trade winds, so they assumed that the  
200 distributions of ZTD are effected by some physical impacts such as terrains and heat  
201 circulation. Compared with the previous discovery, the sawtooth shape in Figure 3a is  
202 more evident, indicating that GZTD2 model incorporates these physical impacts.  
203 Figures 3b and 3c show the global distributions of annual amplitude and semiannual  
204 amplitude respectively, both of which are more uniform in the Southern Hemisphere  
205 than that in the Northern Hemisphere, which is probably due to the fact that most parts  
206 of the Southern Hemisphere are covered by oceans, while the Northern Hemisphere has  
207 many seacoast regions which lead to relatively complex spatial variation.

208 Figure 3d shows the global distribution of diurnal variation amplitudes. It can be  
209 seen that diurnal variation amplitudes are less than 3 mm in most parts of the world, but  
210 up to centimeter in some low-latitude equatorial areas such as Central America, South  
211 America, central Africa and tropical Asia, indicating notable diurnal variations in these  
212 areas. The distribution characteristics of diurnal variation amplitudes is similar to the  
213 results of Jin et al. (2009). So taking these diurnal variations into consideration in  
214 GZTD2 model is quite reasonable and necessary in theory.

215 GZTD2 model only needs doy, UTC time, latitude, longitude and height as input  
216 parameters in practical application. GZTD2 uses equation (2) to derive temporal  
217 parameters  $a_0, a_1, a_2, a_3, a_4, a_5, a_6$ , which are then entered into equation (1)  
218 together with the doy to get the ZTD at MSL. The realization of GZTD2 model is simple  
219 with a few parameters, and the calculation is convenient without inputting any real-time  
220 meteorological parameters. Table 1 summarizes the main improvements and features of  
221 the newly suggested model compared to the GZTD model.



222

**Table 1.** Improvements of GZTD2 with respect to GZTD

	GZTD	GZTD2
Data	Daily average ZTD grid data from GGOS: 2002~2009	ZTD grid data with a resolution of 6 h from GGOS: 2002~2009
Representation	Spherical harmonics up to degree 10 and order 10	Spherical harmonics up to degree 18 and order 18
Temporal variability	Mean, annual, and semi-annual terms	Mean, annual, semi-annual and diurnal terms
Horizontal resolution	About 18 °	About 10 °

223

### 224 3. Validation and Analysis of GZTD2 model

225 To analyze the effectiveness and reliability of the new model and verify its  
 226 accuracy and stability on global scale, as well as to compare it with the GZTD model,  
 227 this section will exploit some data sources to conduct model validation. Two kinds of  
 228 data sources are used here, the first is ZTD grid data from GGOS Atmosphere which is  
 229 not used in modeling. The other is tropospheric product data provided by IGS. The  
 230 accuracy is characterized with the average deviation (Bias) and root mean square (RMS)  
 231 which are usually used for model validation (Yao et al., 2013; Li Wei et al., 2015; Böhm  
 232 et al., 2015). The expressions of Bias and RMS are:

$$233 \quad Bias = \frac{1}{n} \sum_{i=1}^n (ZTD_i^M - ZTD_i^0) \quad (3)$$

$$234 \quad RMS = \sqrt{\frac{1}{n} \sum_{i=1}^n (ZTD_i^M - ZTD_i^0)^2} \quad (4)$$

235 Where  $ZTD_i^M$  is the value estimated by model and  $ZTD_i^0$  is the reference value.

#### 236 3.1 Validation with GGOS Atmosphere ZTD grid data

237 Data provided by GGOS Atmosphere from 2002 to 2009 are involved in modeling,  
 238 so we used the data of 2010 to test it. Since the resolution of ZTD grid data is  $2^\circ \times 2.5^\circ$ ,

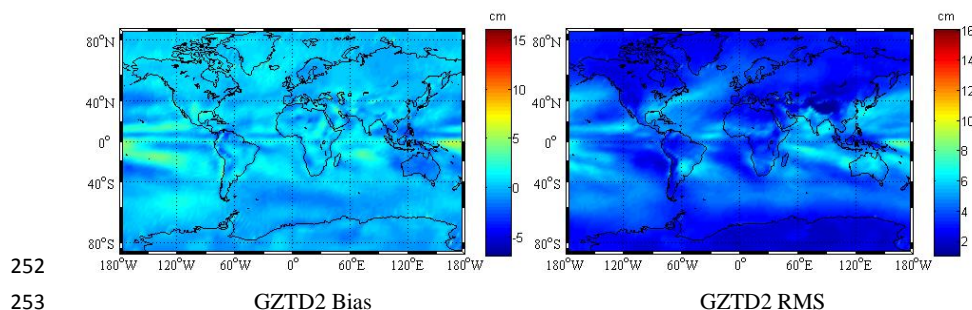


239 the total number of grid points is 13,104. Treating the ZTD data at 0:00, 6:00, 12:00  
 240 and 18:00 UTC of everyday on each grid point as the reference values, we calculated  
 241 the bias and RMS of GZTD2, GZTD, EGNOS, UNB3 and UNB3m models. Statistical  
 242 analyses are shown in Table 2.

243 **Table 2.** Modeling errors of different models validated by GGOS data

	Bias (in cm)			RMS (in cm)		
	Mean	Min	Max	Mean	Min	Max
GZTD2	0.2	-3.7	6.2	3.8	0.9	8.3
GZTD	0.2	-5.4	8.0	4.1	1.1	9.5
UNB3m	3.3	-7.2	16.0	6.4	1.3	16.5
UNB3	4.5	-7.0	16.7	7.0	1.1	16.9
EGNOS	4.5	-9.6	17.7	7.2	1.0	18.1

244 As can be seen from Table 2, for the total 13104 points involved in the global  
 245 validation, GZTD2 model's mean Bias is 0.2 cm with a maximum of 6.2 cm, and the  
 246 average of RMS is 3.8 cm with a maximum of 8.3 cm, significantly better than the  
 247 EGNOS and UNB series models, and the RMS is reduced by 3 mm compared with that  
 248 of GZTD model. UNB3m model's accuracy is about 1 cm better than UNB3 and  
 249 EGNOS models, so we only chose UNB3m as the representative of commonly used  
 250 model in our following comparison analysis. Figure 4 shows the global distributions of  
 251 Bias and RMS of the three models.



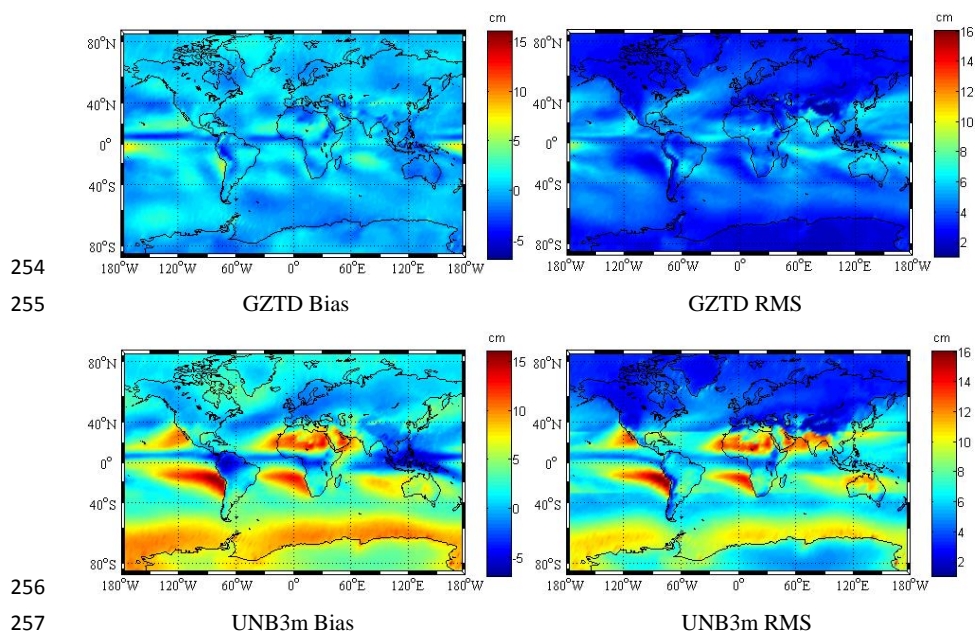


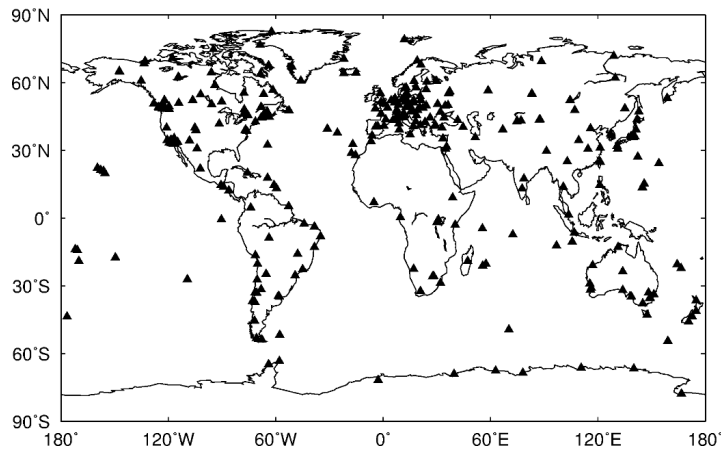
**Figure 4.** Global distribution of Bias and RMS of different models

259 As can be seen from Figure 4, compared with the other two models, the new model  
260 has better accuracy in the world wide scale, and the accuracy of the areas where lager  
261 errors appear improves significantly. Compared with GZTD model, GZTD2 model  
262 improves the accuracy in the equator area. Obviously, all these three models have  
263 suffered large errors in the Pacific Ocean near the equator and Indian Ocean. These  
264 areas are near the equator and may be affected by trade winds and ocean currents, so  
265 the climate change in these areas are more complex compared with other areas,  
266 resulting in difficulty for modelling tropospheric delay. In addition, GZTD2 and GZTD  
267 model are comparable in Northern and Southern Hemispheres, but the UNB3m model's  
268 accuracy is obviously lower in the Southern Hemisphere, this is because the UNB3m  
269 model is based on the assumptions that tropospheric delay is symmetrical with equator  
270 (Leandro et al., 2006). In fact, this assumption is not reasonable enough and the  
271 modeling data source are derived from North America, so the accuracy of the model is  
272 higher in North Hemisphere, especially in Northern America.



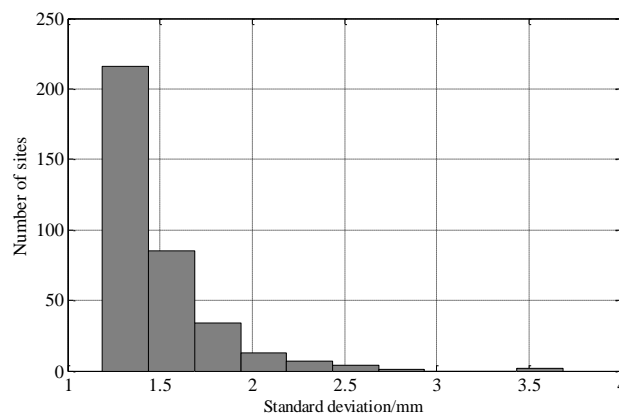
### 273 3.2 Validation with IGS tropospheric delay data

274 IGS has provided final troposphere products with a temporal resolution of 5  
275 minutes since 1998. There are 362 IGS sites selected in 2010 to verify the accuracy of  
276 GZTD2 model, and the distribution of IGS sites is shown in Figure 5. The uncertainties  
277 of the ZTD products are very small (see Figure 5) with a mean value of 1.5 mm,  
278 indicating high quality of the ZTD products. Considering the ZTD products of IGS sites  
279 as true value, we tested and analyzed the ZTD estimates of GZTD2 model, GZTD  
280 model, EGNOS model and UNB series models. The Bias and RMS statistical results  
281 are shown in Table 3.



282  
283

**Figure 5.** Distribution of global IGS sites involved in validation



284  
285

**Figure 6.** Histogram of uncertainty of ZTD at selected IGS sites

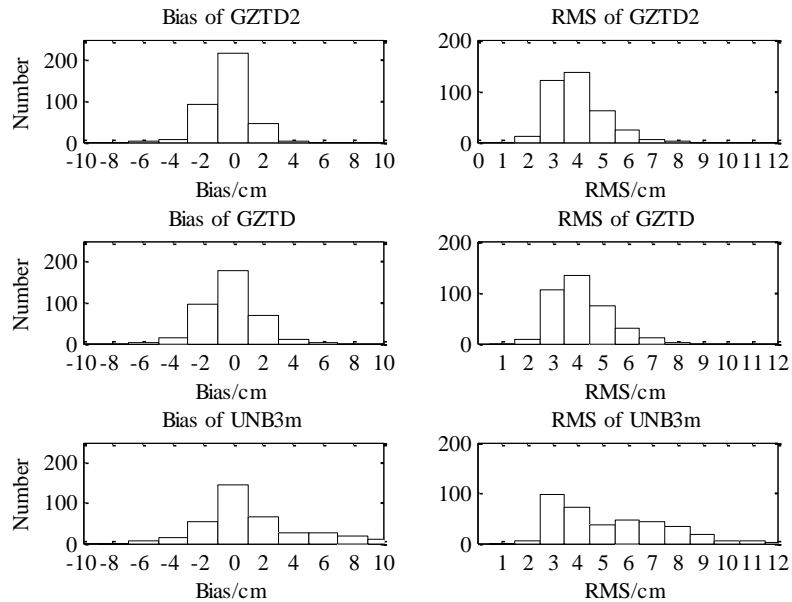


286

**Table 3.** Error of different considered models versus IGS data

	Bias (in cm)			RMS (in cm)		
	Mean	Min	Max	Mean	Min	Max
GZTD2	-0.3	-5.4	3.2	3.9	2.0	8.3
GZTD	-0.3	-6.0	5.1	4.2	2.1	8.5
UNB3m	1.2	-6.7	11.2	5.2	2.4	12.2
UNB3	2.6	-6.5	13.4	5.6	2.3	13.7
EGNOS	2.4	-6.6	15.3	5.7	2.4	12.3

287 As can be seen from Table 3, in terms of the results of accuracy and stability testing  
288 for all IGS sites throughout the year, GZTD2 model performs with the best average  
289 RMS, and then GZTD model followed. Global correction accuracy of the new model  
290 reaches centimeter level: Bias average value is -0.3 cm, average RMS is 3.9 cm.  
291 Compared with GZTD model, the range of Bias of GZTD2 model reduce by 2.4 cm  
292 and the maximum RMS of GZTD2 model decreases by 0.2 cm, indicating that the new  
293 model has a higher stability. Bias and RMS of EGNOS model are very close to those  
294 of UNB3 model and both are worse than UNB3m, which is similar to the results of Li  
295 et al. (2012). To display the correction effects of different models in a more intuitive  
296 way, we computed the distributions of Bias and RMS of all IGS stations. Figure 7 shows  
297 the histograms of Bias and RMS for the three models.

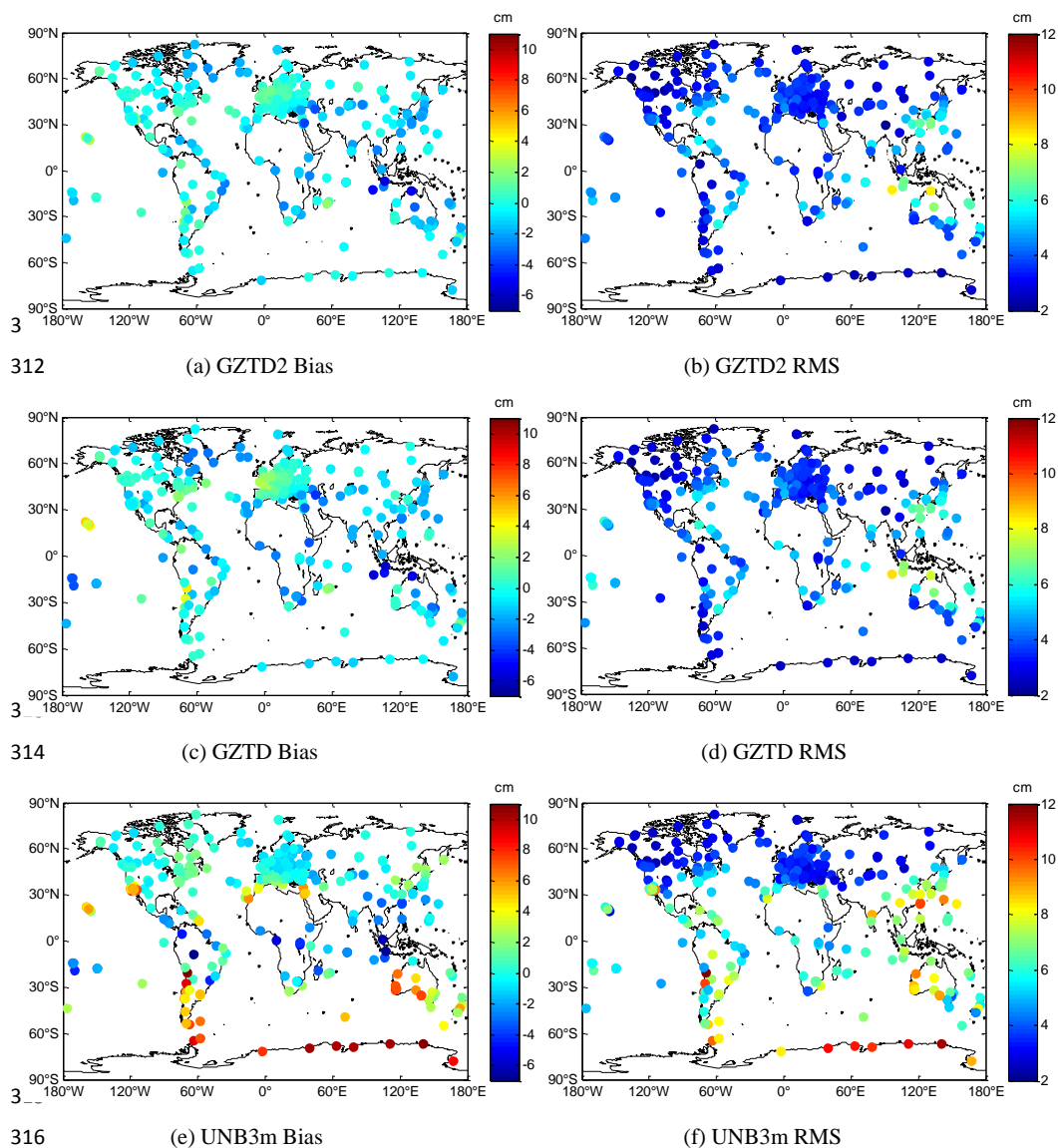


298

299

**Figure 7.** Histograms of Bias and RMS for three models

300 As can be seen from Figure 7, the Bias of GZTD2 model concentrates in range of  
301 [-3cm 3cm], while the main distribution range of the Bias of GZTD model are 1cm  
302 larger, and the Bias for UNB3m is distributed with the range more than 8 cm. It indicates  
303 that GZTD2 model and GZTD model have small systematic deviations compared with  
304 IGS data on a global scale, with the former performing better than the latter, but  
305 problematic systematic deviations exist in the UNB3m model within some special areas.  
306 Figure 7 also shows that the RMS of GZTD2 model is mostly around 4 cm, whose  
307 distribution is more concentrated compared to GZTD model, indicating GZTD2 model  
308 has higher stability than GZTD. The RMS of UNB3m model are mainly around 5 cm  
309 and exceed 9 cm at many sites, which further suggests the existence of systematic  
310 deviations in certain areas in the UNB3m model.

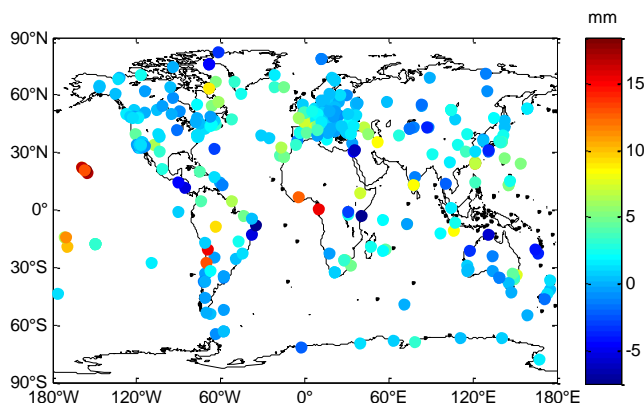


317 **Figure 8.** Global distributions of Bias and RMS for different models

318 To further analyze the accuracy of the different models varying with location,  
319 Figure 8 shows the global distributions of Bias and RMS calculated from different  
320 models for IGS sites. As can be seen from Figure 8, GZTD2 and GZTD model largely  
321 eliminate the effects caused by latitude and longitude variations, and the former is more  
322 stable than the latter in terms of global distribution of Bias and RMS in spite of a few  
323 sites with relative large error, of which most sites are located in the ocean and seacoast



324 areas. A more clear comparison in terms of RMS between GZTD and GZTD2 is shown  
325 in Figure 9. The reduce for RMS can be found at most sites (the number is 273) when  
326 moving from GZTD to GZTD2, which account for 75.4% of all sites. The significant  
327 improvements of RMS are found at the sites in low-latitude areas such as Pacific Ocean,  
328 South America coast and West Africa coast where the diurnal variations are notable  
329 (see Figure 3d). This result proves the reasonability of adding diurnal variations in  
330 GZTD2. For UNB3m model, as it is presented in Figure 8 Biases are negative in most  
331 parts of the Northern Hemisphere and positive in most parts of the Southern  
332 Hemisphere with significantly larger deviations, and RMS are smaller for areas in the  
333 latitudes higher than 30 degrees, again suggesting that the correction effect of UNB3m  
334 model is regional.

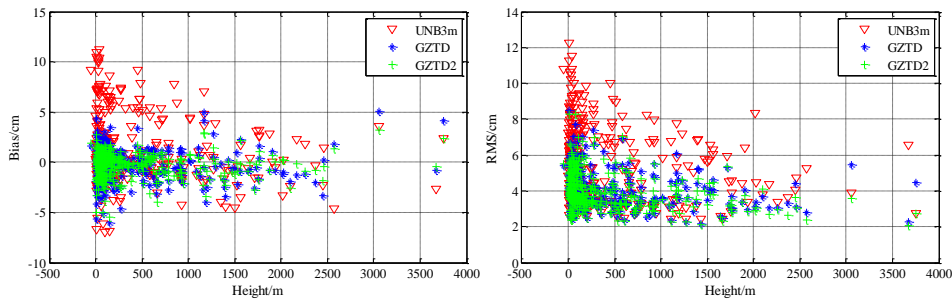


335  
336 **Figure 9.** Global distribution of the difference between GZTD's RMS and GZTD2's RMS (GZTD's  
337 RMS minus GZTD2's RMS)

338 Figure 10 shows the global distribution of Bias and RMS with respect to height  
339 for GZTD2 model, GZTD model and UNB3m model. As can be seen, the Bias and  
340 RMS are larger with height less than 500 m for all three models. Between 500m and  
341 2000m height, the Bias and RMS of GZTD model and GZTD2 model perform better  
342 than that of UNB3m model, and the overall correction effects of the GZTD and GZTD2  
343 model are also better than the latter. Due to the same exponential function and reducing  
344 constant for height, the distribution patterns of the Bias and RMS of GZTD and GZTD2  
345 model with respect to height are roughly similar, but the latter is obviously superior to



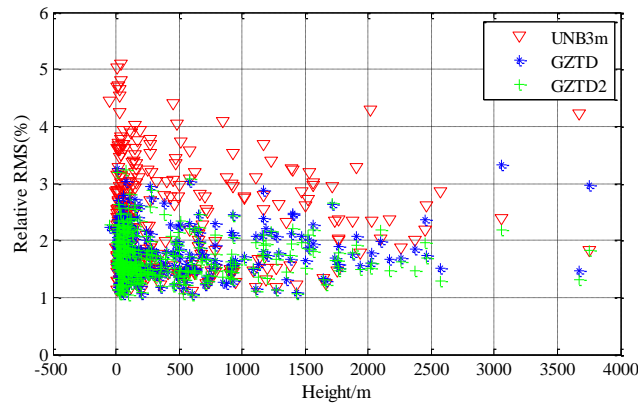
346 the former.



347

348 **Figure 10.** Global distributions of Bias and RMS for different models with respect to height

349 For a more comprehensive analysis of the relationship between model stability and  
350 height, Figure 11 presents the global distribution of relative RMS for three models with  
351 respect to height. The relative RMS is the ratio of the RMS to the annual mean ZTD at  
352 the site. Basically, a relative accuracy between 1% and 2.5% can usually be stated for  
353 the majority of the sites from GZTD2 model, and the relative accuracy is less than 3%  
354 for GZTD model, showing that both perform better than UNB3m model.



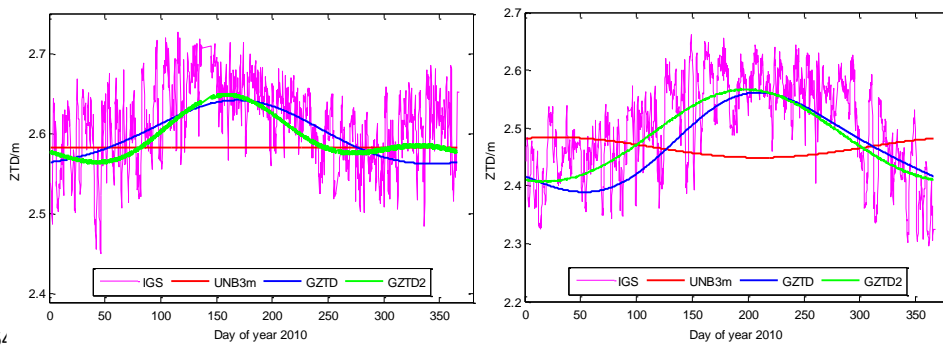
355

356 **Figure 11.** Relative RMS for different models with respect to height

357 Figure 12 illustrates the comparisons between IGS ZTD data and ZTDs  
358 determined by UNB3m, GZTD and GZTD2 models over the year 2010 at site KOUR  
359 and TWTF. During the whole year 2010, the ZTD values estimated by GZTD2 model  
360 show the best agreement with the IGS data, which are better than that of GZTD model  
361 without diurnal terms. The ZTDs determined by UNB3m model vary slightly  
362 throughout the year 2010, thus resulting in poor performance. The results in Figure 12



363 indicates that GZTD2 model has a temporal stability for correction accuracy.



364  
365 **Figure 12.** ZTDs at site KOUR (5.3 °N, 52.8 °W, 9.5m; left) and TWTF (24.9 °N, 121.2 °E, 189.9m;  
366 right) as provided by IGS and as estimated by different models over year 2010

367 From the above analysis, we can conclude that the overall accuracy of GZTD2  
368 model is up to centimeter level. GZTD2 model is obviously superior to other commonly  
369 used models in terms of Bias and RMS, and the accuracy improve significantly  
370 compared with GZTD model, thus performing a higher reliability and stability.

371

## 372 4 Conclusions

373 In this paper, we used time series data of global tropospheric zenith delays  
374 provided by GGOS Atmosphere, and considered the diurnal variation in the ZTD based  
375 on the GZTD model, and adopted a modified expansion function, and ultimately  
376 developed an improved model named GZTD2. We conducted external validation  
377 testing with ZTD grid data which was not involved in modeling, and IGS tropospheric  
378 product. The testing results of ZTD grid data reflect the global precision and stability  
379 for GZTD2 model at four moments each day, and the global average Bias and RMS for  
380 GZTD2 model are 0.2 cm and 3.8 cm respectively; the global average Bias is  
381 comparable to that of GZTD model, but the global average RMS has been reduced by  
382 3 mm; the Bias and RMS are far better than EGNOS model and the UNB series models.  
383 The testing results of global IGS tropospheric product show the Bias and RMS for  
384 GZTD2 model are -0.3 cm and 3.9 cm, superior to that of GZTD (-0.3 cm and 4.2 cm),



385 indicating higher accuracy and reliability compared to the EGNOS model and the UNB  
386 series models.

387 Overall, compared to GZTD model, GZTD2 model improves the temporal  
388 resolution and spatial resolution by considering diurnal periodic variations and  
389 modifying the expansion function, further completing and optimizing the theory of  
390 model establishment. The reliability and stability for GZTD2 model are much better  
391 than other commonly used models. However, like other empirical models such as  
392 UNB3m, GZTD2 model would be inaccurate in extreme weather events. Saastamoinen  
393 model is recommended if the real-time meteorological observations are available under  
394 extreme weather events. Moreover, GZTD2 model doesn't consider the semidiurnal  
395 variations due to the temporal resolution of GGOS data. In order to build a global  
396 tropospheric model with high accuracy, ZTD data with high quality and resolution are  
397 required, and the diurnal and semidiurnal variations as well as the subtle secular  
398 variation trend of ZTD need more detailed and further study.

399

400 *Acknowledgements* The authors would like to express gratitude toward GGOS  
401 Atmosphere for providing related data. Great appreciation also goes to IGS for their  
402 data supporting of reference tropospheric product. This research was supported by the  
403 National Natural Science Foundation of China (41174012; 41274022) and The  
404 National High Technology Research and Development Program of China  
405 (2013AA122502) and the Fundamental Research Funds for the Central Universities  
406 (2014214020202) and the Surveying and Mapping Basic Research Program of  
407 National Administration of Surveying, Mapping and Geoinformation (13-02-09).

408

## 409 **References**

- 410 Black H D (1978). An easily implemented algorithm for the tropospheric range correction. *Journal*  
411 *of Geophysical Research: Solid Earth (1978–2012)*, **83**(B4), 1825-1828.
- 412 Böh m, J., Heinkelmann, R., & Schuh, H. (2007). Short note: a global model of pressure and



- 413 temperature for geodetic applications. *Journal of Geodesy*, **81**(10), 679-683.
- 414 B öhm, J., & Schuh, H. (eds.) (2013). *Atmospheric Effects in Space Geodesy*, Springer Verlag, ISBN  
415 978-3-642-36931-5.
- 416 B öhm, J., Möller, G., Schindelegger, M., Pain, G., & Weber, R. (2015). Development of an improved  
417 empirical model for slant delays in the troposphere (GPT2w). *GPS Solutions*, *19*(3), 433-441.
- 418 Byun, S. H., & Bar-Sever, Y. E. (2009). A new type of troposphere zenith path delay product of the  
419 international GNSS service. *Journal of Geodesy*, **83**(3-4), 1-7.
- 420 Collins J P, Langley R B(1997). *A tropospheric delay model for the user of the wide area*  
421 *augmentation system. Department of Geodesy and Geomatics Engineering*, University of New  
422 Brunswick.
- 423 Collins, J. P., & Langley, R. (1998, September). The residual tropospheric propagation delay: How  
424 bad can it get? In *PROCEEDINGS OF ION GPS* (Vol. 11, pp. 729-738). INSTITUTE OF  
425 NAVIGATION.
- 426 Dodson A H, Chen W, Baker H C, Penna N T, Roberts G W, Jeans R J, Westbrook J(1999).  
427 Assessment of EGNOS tropospheric correction model. In *Proceedings of the 12th International*  
428 *Technical Meeting of the Satellite Division of The Institute of Navigation (ION GPS 1999)* (pp.  
429 1401-1408).
- 430 Hopfield H S (1969). Two - quartic tropospheric refractivity profile for correcting satellite data.  
431 *Journal of Geophysical research*, **74**(18), 4487-4499.
- 432 Jin, S., Park, J. U., Cho, J. H., & Park, P. H. (2007). Seasonal variability of GPS - derived zenith  
433 tropospheric delay (1994 - 2006) and climate implications. *Journal of Geophysical Research:*  
434 *Atmospheres (1984 - 2012)*, 112(D9).
- 435 Jin, S., Luo, O. F., & Gleason, S. (2009). Characterization of diurnal cycles in ZTD from a decade  
436 of global GPS observations. *Journal of Geodesy*, **83**(6), 537-545.
- 437 Krueger E, Schueler T, Hein G W, Martellucci A, Blarmino G(2004, May). Galileo tropospheric  
438 correction approaches developed within GSTB-V1. In *Proc. ENC-GNSS*.
- 439 Krueger E, Schueler T, Arbesser-Rastburg B(2005). The standard tropospheric correction model for  
440 the European satellite navigation system Galileo. *Proc. General Assembly URSI*.
- 441 Lagler, K., Schindelegger, M., B öhm, J., Kr ásn á H., & Nilsson, T. (2013). GPT2: Empirical slant  
442 delay model for radio space geodetic techniques. *Geophysical research letters*, *40*(6), 1069-1073.



- 443 Leandro R, Santos M C, Langley R B(2006, January). UNB neutral atmosphere models:  
444 development and performance. In *ION NTM* (pp. 18-20).
- 445 Leandro R F, Langley R B, Santos M C(2008). UNB3m\_pack: a neutral atmosphere delay package  
446 for radiometric space techniques. *GPS Solutions*, **12**(1), 65-70.
- 447 Li W, Yuan Y B, Ou J K, Li H, Li Z S(2012). A new global zenith tropospheric delay model IGGtrop  
448 for GNSS applications. *Chinese Science Bulletin*, **57**(17), 2132-2139.
- 449 Li, W., Yuan, Y., Ou, J., Chai, Y., Li, Z., Liou, Y. A., & Wang, N. (2015). New versions of the  
450 BDS/GNSS zenith tropospheric delay model IGGtrop. *Journal of Geodesy*, **89**(1), 73-80.
- 451 Möller, G., Weber, R., & Böhm, J. (2014). Improved troposphere blind models based on numerical  
452 weather data. *Navigation*, **61**(3), 203-211.
- 453 Penna N, Dodson A, Chen W(2001). Assessment of EGNOS tropospheric correction model. *The*  
454 *Journal of Navigation*, **54**(01), 37-55.
- 455 Saastamoinen J (1973). Contributions to the theory of atmospheric refraction. *Bulletin G éod ésique*  
456 *(1946-1975)*, **107**(1), 13-34.
- 457 Schüler T (2014). The TropGrid2 standard tropospheric correction model. *GPS solutions*, **18**(1),  
458 123-131.
- 459 Ueno M, Hoshino K, Matsunaga K, Kawai M, Nakao H, Langley R B, Bisnath S B (2001, January).  
460 Assessment of atmospheric delay correction models for the Japanese MSAS. In *Proceedings of*  
461 *the 14th International Technical Meeting of the Satellite Division of The Institute of Navigation*  
462 *(ION GPS 2001)* (pp. 2341-2350).
- 463 Uppala S M, K ällberg P W, Simmons A J, Andrae U, Bechtold V, Fiorino M, ... , Woollen J (2005).  
464 The ERA - 40 re - analysis. *Quarterly Journal of the Royal Meteorological Society*, **131**(612),  
465 2961-3012.
- 466 Yao Y B, He C Y, Zhang B, Xu C Q(2013). A new global zenith tropospheric delay model GZTD.  
467 *Chinese Journal of Geophysics-Chinese Edition*, **56**(7), 2218-2227,doi:10.6038/cjg20130709